

Testing the ACA Phase Correction Scheme using the SMA

Satoki MATSUSHITA^{1,2} and Yu-Lin CHEN^{1,3,4}

¹*Institute of Astronomy and Astrophysics, Academia Sinica, P.O. Box 23-141, Taipei 10617, Taiwan, R.O.C.
satoki@asiaa.sinica.edu.tw*

²*Joint ALMA Office, Av. El Golf 40, Piso 18, Las Condes, Santiago, Chile*

³*Department of Physics, National Taiwan University, No. 1, Sec. 4, Roosevelt Road, Taipei 10617, Taiwan, R.O.C.*

⁴*Taipei County Yong-Ho Junior High School, No. 111, Guozhong Rd., Yonghe City, Taipei County 234, Taiwan, R.O.C.*

(Received 2010 February 23; accepted 2010 May 17)

Abstract

We conducted the observational tests of a phase correction scheme for the Atacama Compact Array (ACA) of the Atacama Large Millimeter and submillimeter Array (ALMA) using the Submillimeter Array (SMA). Interferometers at millimeter- and submillimeter-wave are highly affected by the refraction induced by water vapor in the troposphere, which results as phase fluctuations. The ACA is planning to compensate the atmospheric phase fluctuations using the phase information of the outermost antennas with interpolating to the inner antennas by creating a phase screen. The interpolation and extrapolation phase correction schemes using phase screens are tested with the SMA to study how effective these schemes are. We produce a plane of a wavefront (phase screen) from the phase information of three antennas for each integration, and this phase screen is used for the interpolation and extrapolation of the phases of inner and outer antennas, respectively. The interpolation scheme obtains apparently improved results, suggesting that the ACA phase correction scheme will work well. On the other hand, the extrapolation scheme often does not improve the results. After the extrapolation, unexpectedly large phase fluctuations show up to the antennas at the distance of ~ 140 m away from the center of the three reference antennas. These direction vectors are almost perpendicular to the wind direction, suggesting that the phase fluctuations can be well explained by the frozen phase screen.

Key words: atmospheric effects — submillimeter — techniques: high angular resolution — techniques: interferometric

1. Introduction

The Atacama Large Millimeter and submillimeter Array (ALMA), the largest millimeter and submillimeter interferometer ever built, is currently under construction in the northern Chile with the collaboration between East Asia, Europe, and North America (Wootten & Thompson 2009). The ALMA is composed of up to eighty high-precision antennas, located on the Chajnantor plain of the Chilean Andes in the District of San Pedro de Atacama, 5000 m above sea level. The ALMA covers the wavelength range from 0.3 mm to 9 mm with an angular resolution of up to $0''.004$. The Atacama Compact Array (ACA) is designed to improve the short baseline coverage of the ALMA, especially for the observations of extended structures at submillimeter wavelength (Iguchi et al. 2009). The ACA consists of four 12 m telescopes to obtain the single-dish data and twelve 7 m telescopes to obtain short baseline interferometric data.

However, ground-base astronomical observations in the millimeter and submillimeter ranges are strongly affected by the fluctuation of the tropospheric water vapor distribution (e.g., Thompson et al. 2001). Therefore, the correction of phase fluctuations due to the spatial and temporal variations of the tropospheric water vapor content is extremely important in millimeter and submil-

limeter interferometry. Several kinds of techniques have been proposed and performed for reducing phase fluctuations in millimeter and submillimeter interferometry (see Carilli & Holdaway 1999 for a review), such as fast switching phase calibration (Holdaway 1992; Holdaway & Owen 1995; Carilli & Holdaway 1997; Morita et al. 2000), paired array phase calibration (Holdaway 1992; Carilli et al. 1996; Asaki et al. 1996; Asaki et al. 1998), and radiometric phase calibration (Lay 1997; Carilli et al. 1998; Carilli & Holdaway 1999; Marvel & Woody 1998; Delgado et al. 2000; Wiedner et al. 2001; Matsushita et al. 2002). Although the ALMA site is one of the best sites for the millimeter and submillimeter astronomy (Matsuo et al. 1998; Matsushita et al. 1999; Paine et al. 2000; Matsushita & Matsuo 2003), atmosphere in this area is often affected by the phase fluctuations due to water vapor (Radford et al. 1996; Holdaway et al. 1997; Butler et al. 2001). The phase correction methods for the ALMA and the ACA are therefore highly needed to be considered and tested.

Asaki et al. (2005) conducted a series of simulations of a phase correction scheme for the ACA using water vapor radiometers (WVRs). The WVRs can measure the tropospheric water vapor content directly with observing a water vapor line in centimeter or millimeter wavelength. In the proposed ACA phase calibration scheme, the WVRs are attached to the 12 m antennas at the four corners of

the twelve 7 m array (hereafter we call this as the reference rectangle). The changes of the tropospheric water vapor content aloft measured with the WVRs is transferred into the excess path lengths of the arriving radio waves. The excess path lengths measured at the four corners of the reference rectangle are then fitted to a simple two-dimensional slope or a screen. Then the phases of the antennas inside the reference rectangle can be compensated and calibrated. Their simulation succeeded to compensate the atmospheric phase well, which strongly support the use of the proposed phase correction scheme.

To confirm this simulation study observationally and discuss further, we performed the proposed phase correction scheme for the ACA using the Submillimeter Array (SMA; Ho et al. 2004). Here we present measurements with the SMA at 230 GHz, analyze the datasets under the proposed scheme, and discuss the results of the corrected phase variations. Our experiment is to clarify how effectively the proposed compensation scheme works under the conditions of the real atmosphere. We construct a reference triangle composed of three antennas, and make a flat phase plane or a screen with observing a strong point source (section 2). The phases of antennas inside the reference triangle can be interpolated, while the phases of antennas outside can be extrapolated. We then compare the observed and the predicted phases of the point source. Standard deviations and temporal structure functions of the observed (uncorrected) and the corrected phases are also compared (section 3). Finally, we discuss the usefulness of the interpolation and extrapolation phase correction schemes using a phase screen, and also discuss the validity of the “frozen-flow” hypothesis (section 4).

2. Measurements and Data Reduction

The purpose of our experiment is to investigate observationally the proposed phase compensation method for the ACA using the SMA. The reasons of using the SMA for this experiment are that the SMA is the interferometer operating at submillimeter wavelength, which is the same as the ACA, and that the antenna configuration of the array is applicable for this experiment. The ACA uses the WVRs for the phase compensation, but for this experiment using the SMA, since the SMA does not have WVRs, we observed a strong point source to measure the phase directly to perform the proposed ACA phase compensation method.

2.1. Measurements

The measurements were carried out on August 26, 2004 using all eight antennas of the SMA on Mauna Kea in Hawaii, and on September 7, 2004 using seven antennas (the antenna 8 was not used in this measurement). The antenna configuration is depicted in figure 1. The shortest and the longest baseline lengths are 11.6 m (antenna 1 to antenna 8) and 179.2 m (antenna 4 to antenna 6), respectively. The measurements were performed at 240.0 GHz for the August 26, 2004 measurement and 230.5 GHz for the September 7, 2004 measurement (both frequencies are

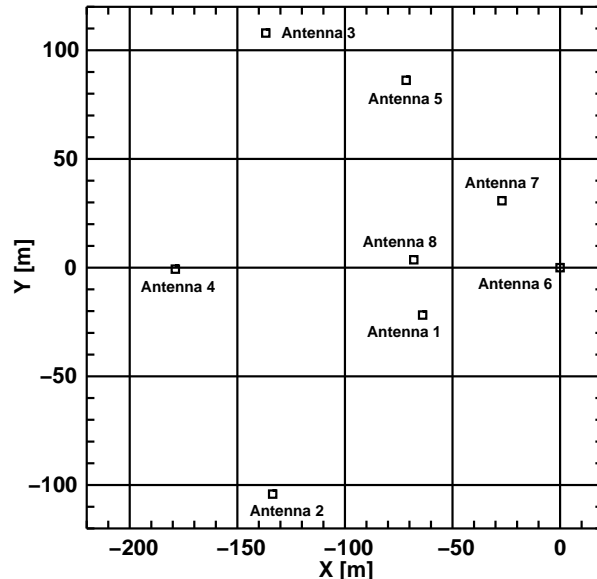


Fig. 1. Configuration of all eight antennas of the SMA at the observations.

at the upper side band). Correlator bandwidth in both measurements was 2 GHz for each side band. We observed B1921 – 293 (J1924 – 291) in both days for 1.157 and 0.469 hours, respectively, with the integration time for one data point (one integration number) of 5.16 seconds. The integration number is the number of our data recorded every integration time since the measurements started, and the ranges of the integration number for the target source turned to be 2321 – 3128 and 140 – 467 for the August 26 and September 7 measurements, respectively. The 230 GHz flux density of this source at the time was about 6 Jy, strong enough to detect in one integration with high signal-to-noise ratio. The data were stored in the SMA data archive directories 040826_01:23:23 and 040907_05:22:09. Hereafter we call the former dataset as “040826” and the latter “040907”.

2.2. Data Reduction

2.2.1. Calibration

We reduced the data using the Owens Valley Radio Observatory software package MIR adopted for the SMA. We only used the upper side band data. The data were calibrated based on the antenna-base calibration. We confirmed that all the final results did not change with the reference antennas in the antenna-base calibration.

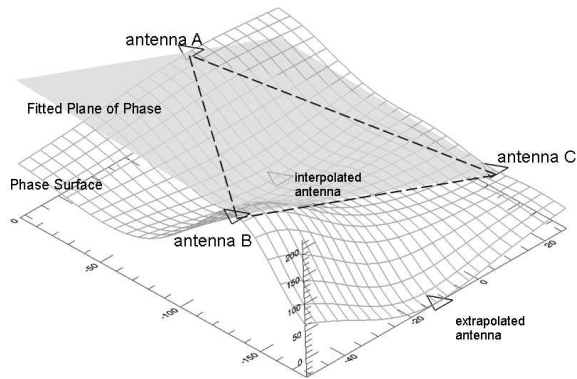
2.2.2. Construction of a Phase Screen

Here we explain the procedure to construct a phase screen using a reference triangle and the comparison between the observed and estimated phases. The schematic diagram is depicted in figure 2.

We first consider a reference triangle composed of three antennas located at the outer periphery of the antenna configuration (antennas A, B, and C in figure 2). Then, a plane of phase or a phase screen through these three antennas can be constructed and computed at each in-

Table 1. Configurations of reference triangles and interpolated and extrapolated antennas inside and outside the triangles.

Reference Antennas	Datasets			
	040826		040907	
	Interpolated Antenna(s)	Extrapolated Antennas	Interpolated Antenna(s)	Extrapolated Antennas
[2, 3, 6]	1, 8	4, 5, 7	1	4, 5, 7
[2, 4, 5]	—	1, 3, 6, 7, 8	—	1, 3, 6, 7
[2, 4, 6]	1	3, 5, 7, 8	1	3, 5, 7
[2, 4, 7]	8	1, 3, 5, 6	—	1, 3, 5, 6
[2, 5, 6]	1, 7, 8	3, 4	1, 7	3, 4
[3, 4, 6]	8	1, 2, 5, 7	—	1, 2, 5, 7
[4, 5, 6]	7, 8	1, 2, 3	7	1, 2, 3

**Fig. 2.** Schematic diagram of a reference triangle with three antennas (A, B, and C) and a constructed phase screen. Interpolated and extrapolated antennas are also shown.

tegration (data point). Note that since the geometrical delay is taken into account at the correlation process (at the SMA backend), we do not need to consider the effect of the antenna altitude differences. In addition, we consider an antenna-base large timescale (> 20 minutes) phase drift as an instrumental phase drift, so we subtract this phase drift with second order polynomial fitting from the data (this kind of large timescale phase drift will be taken out by the phase calibration anyway in the real astronomical observations). From this phase screen, interpolations and extrapolations are conducted to predict phases at each antenna position inside and outside the reference triangle, respectively. We then compare the observed phases with our interpolated and extrapolated phases.

We performed seven different configurations of reference triangles to interpolate and extrapolate the phases of antennas inside and outside the triangle, respectively. The configurations of all the reference triangles we calculated are summarized in table 1. For example, the reference antennas [2, 3, 6] means that we construct phase screens with the coordinates and the observed phases of three antennas 2, 3, and 6.

3. Results

3.1. Comparisons between Observed, Interpolated, Extrapolated, and Residual Phase Fluctuations

First, we show the examples of the phase fluctuation plots of the observed data after the antenna-base gain calibration, and of the interpolated or extrapolated data estimated from a reference triangle for each interpolated or extrapolated antenna in figures 3 and 4. Figure 3 is the plots for the dataset 040826 with the antenna-base gain calibration referring the antenna 2, and with the reference triangle of [2, 3, 6] as an example. Plots in the left and right columns display the results of the interpolated and the extrapolated antennas, respectively. Figure 4 is the same plots, but for the dataset 040907. We also overplotted the subtracted (residual) phase fluctuation plots in the same figures, which are calculated as follows:

$$\begin{aligned}
 & [\text{subtracted (residual) phase}] \\
 &= [\text{observed antenna base gain calibrated phase}] \\
 &\quad - [\text{interpolated or extrapolated phase}]. \tag{1}
 \end{aligned}$$

The subtracted phase tells us how different between the observed and our estimated interpolated or extrapolated phases are, namely how effective our phase correction is.

To evaluate the effectiveness of the phase correction quantitatively, we calculate the standard deviation of our observed, interpolated/extrapolated, and subtracted phase fluctuations, and shown in each plot of figures 3 and 4. It appears that the interpolation scheme leads to smaller residual phases, while the extrapolation scheme does not always improve the phase fluctuations.

It is worth to note that the observed phase fluctuation of the dataset 040826 is more stable than that of the dataset 040907, and the phase fluctuation decreased in both cases (for the interpolation results). In addition, even within one dataset, the degree of phase fluctuation and that of phase correction change drastically. For example, in the dataset 040826, the phase fluctuation of the subtracted phase changes a lot between the integration number ranges of 2321 – 2799 and 2800 – 3128; the standard deviation of the phase fluctuation improved a bit for the former case, but improved a lot for the latter case (figure 3). This suggests that under whatever weather condition (as far as there is no 2π ambiguity; see the next

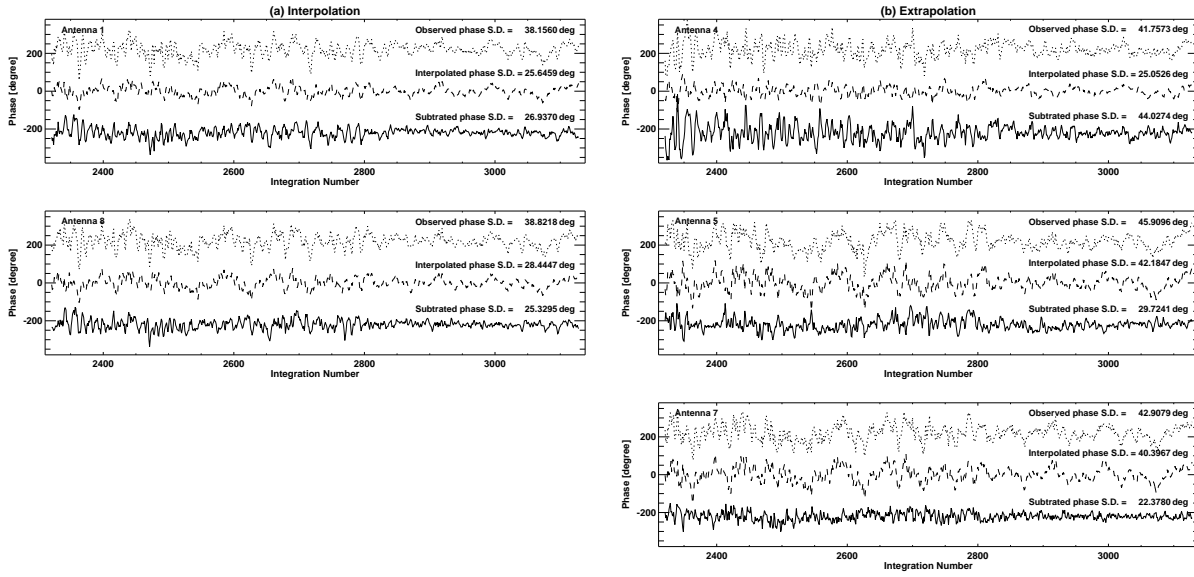


Fig. 3. The time series plots of various phases from the dataset 040826 between the integration number 2321 – 3128 with the reference triangle [2, 3, 6]. The dotted curves show the observed antenna-base gain calibrated data, the dashed curves show the interpolated or extrapolated data, and the solid curves trace the subtracted data between the observed and modeled (interpolated/extrapolated) phases, namely the residual (phase corrected) data. The observed and subtracted data curves are arbitrary offset not to overlap each other. The standard deviation (S.D.) of the phase fluctuations over the integration time range for each curve are shown in the plots. The interpolated results always have better results, while the extrapolated results do not always have in this example. (a) The interpolation results for the antennas 1 and 8. (b) The extrapolation results for the antennas 4, 5, and 7.

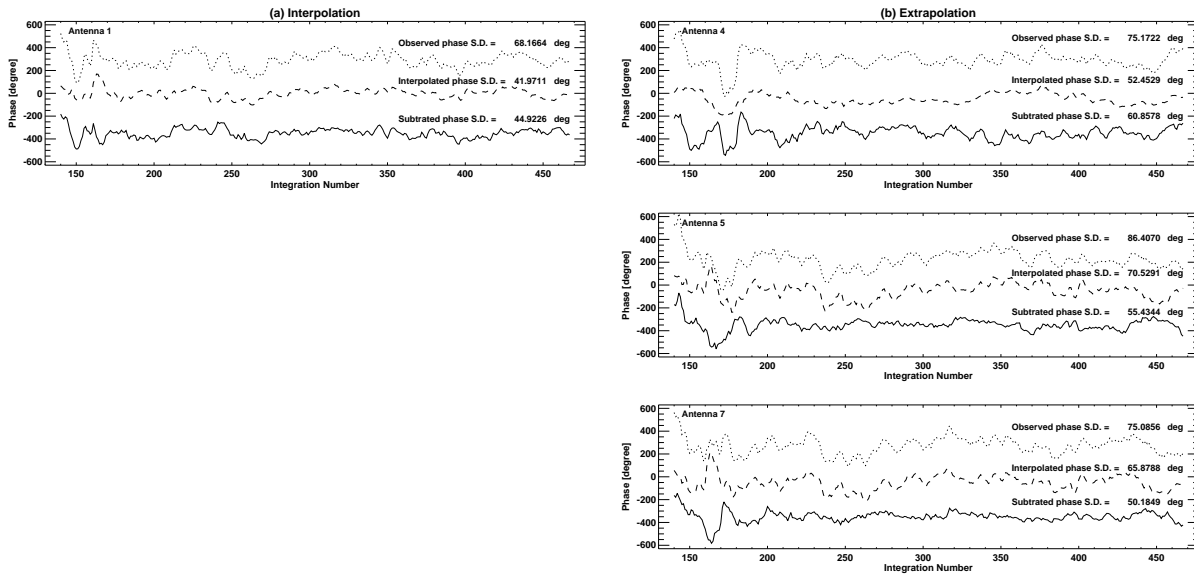


Fig. 4. The time series plots of various phases from the dataset 040907 between the integration number 140 – 467 with the reference triangle [2, 3, 6]. Other information is the same as in figure 3. (a) The interpolation results for the antenna 1. (b) The extrapolation results for the antennas 4, 5, and 7.

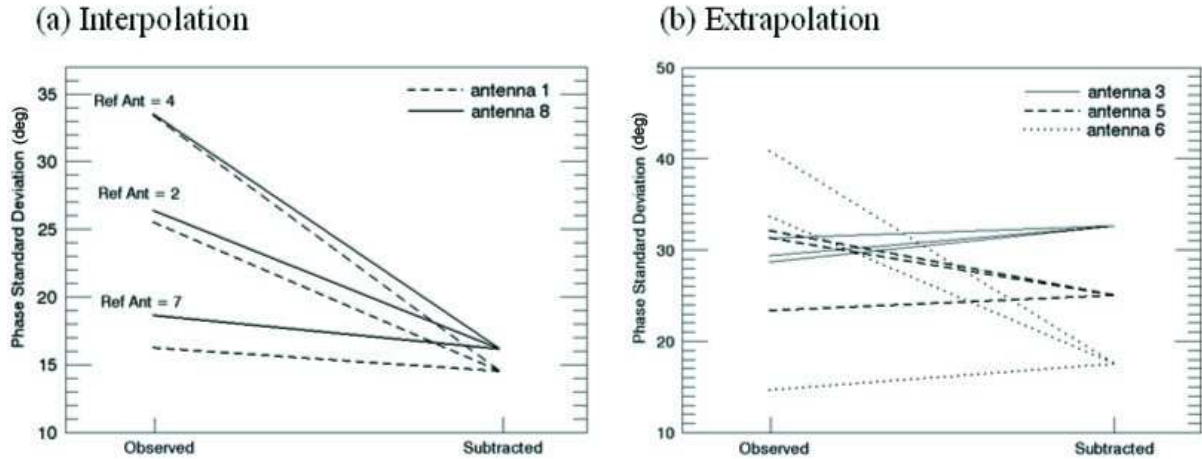


Fig. 5. Observed and subtracted phase standard deviation under the same reference triangle [2, 4, 7] and the same integration number range 2800 – 3128, but different reference antennas for the antenna-based gain calibration. Data calibrated with different reference antennas have different observed phase standard deviation, but they all have identical phase standard deviations after the phase subtraction. (a) The interpolation results for antennas 1 and 8. (b) The extrapolation results for antennas 3, 5, and 6.

Table 2. Two datasets divided into two parts based on their observed phase variations.

	Integration Number Range	
	040826	040907
Earlier Part	2321 – 2799	140 – 199
Later Part	2800 – 3128	200 – 467

paragraph), the interpolation phase correction works.

When the phase fluctuation is too large, this phase correction does not work effectively in either interpolation or extrapolation. This effect is obvious in the integration number range of 140 – 199 of the 040907 dataset. We find out that the main reason of this failure is due to the 2π ambiguity of the observed phase. Interferometers can measure the phase only within $\pm\pi$, so if the phase fluctuates largely, the observed phase wraps within $\pm\pi$, and it is difficult to recover the actual phase fluctuations larger than $\pm\pi$.

Hereafter, we separate each dataset into two integration number ranges, and these are shown in table 2. We divided both of our two datasets into earlier and later parts. The foreparts of 040826 and 040907 are the integration number ranges of 2321 – 2799 and 140 – 199, respectively, which have larger variations on phase than the later parts of 2800 – 3128 and 200 – 467.

3.2. Re-Define the Phase: Phase Refers to the Center of the Reference Triangle

The degree of the improvement of the phase fluctuation after the phase correction, however, depends on the reference antenna of the antenna-based gain calibration. If the interpolated antenna is close to the reference antenna, the improvement of the phase fluctuation is small, but if the interpolated antenna is far from the reference antenna, the improvement of the phase fluctuation is large. In addition, the final results, namely the residual phase fluctuations,

do not depend on reference antennas. In figure 5, we show examples of the observed and subtracted phases with different reference antennas for the antenna-based gain calibration under the same reference triangle [2, 4, 7]. As can be seen, the standard deviations of the observed phases largely depend on the reference antennas, but that of the subtracted phases converges into one. Furthermore, in case of the interpolation scheme (figure 5a), subtracted phases improve in all the three reference antenna cases, but in case of the extrapolation scheme (figure 5b), subtracted phases improve in some reference antenna cases and some do not.

These can be explained as follows: Observed phase with the antenna X using the antenna r as the reference antenna for the antenna-based gain calibration, ϕ_{Xr} , can be expressed as

$$\phi_{Xr} = \phi_X - \phi_r, \quad (2)$$

where ϕ_X and ϕ_r are the absolute phase observed with the antenna X and the reference antenna r . The estimated phase with interpolation or extrapolation, ϕ'_{Xr} , can be expressed as

$$\phi'_{Xr} = \phi_{X,estimated} - \phi_r, \quad (3)$$

where $\phi_{X,estimated}$ is the absolute estimated phase at the antenna X. Both of the above equations depend on the absolute phase of the reference antenna r . On the other hand, the final result, which is the subtraction between the observed and the estimated phases, is expressed as

$$\begin{aligned} \phi_{Xr} - \phi'_{Xr} &= \phi_X - \phi_r - (\phi_{X,estimated} - \phi_r) \\ &= \phi_X - \phi_{X,estimated}, \end{aligned} \quad (4)$$

which does not depend on the reference antenna, and therefore the subtracted phase converged into one result, as shown in figure 5.

To evaluate the effectiveness of the phase correction more quantitatively, we re-define the phase to that refers

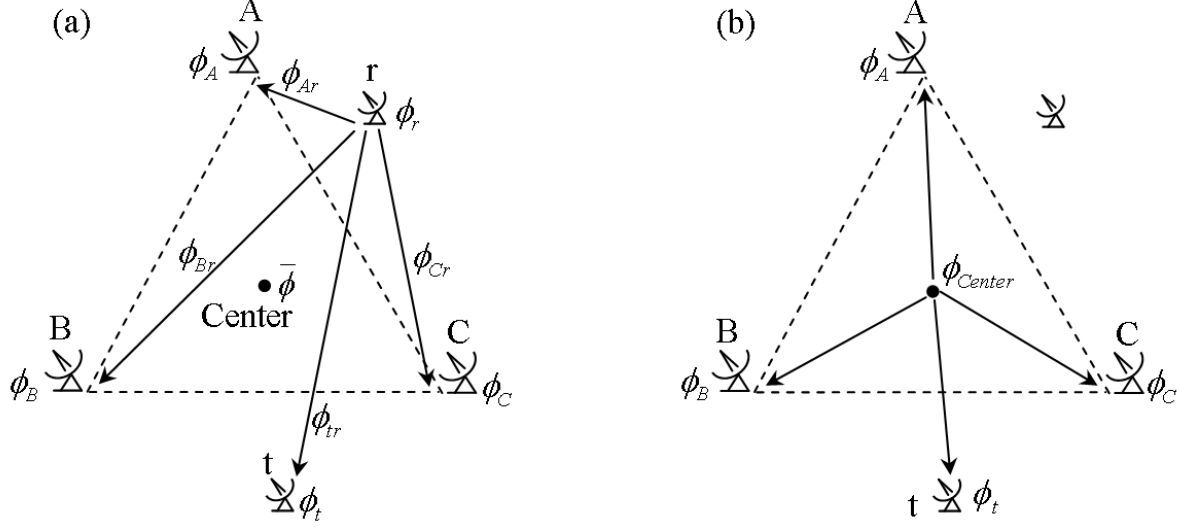


Fig. 6. The simple diagrams of the phase conversion from (a) the observed phase to (b) the phase measured from the center of the reference triangle. The three antennas A, B, and C are located at the corners of the reference triangle. The reference antenna for the antenna-base gain calibration, r , and the target antenna whose phase is to be corrected, t , are also shown in the plots.

to the center of the reference triangle. Consider a reference triangle composed of three antennas, A, B, and C (figure 6a). The observed phases for these three antennas after the antenna-base gain calibration using the reference antenna r , ϕ_{Ar} , ϕ_{Br} , and ϕ_{Cr} , can be expressed as

$$\phi_{Ar} = \phi_A - \phi_r, \quad (5)$$

$$\phi_{Br} = \phi_B - \phi_r, \quad (6)$$

$$\phi_{Cr} = \phi_C - \phi_r, \quad (7)$$

where ϕ_A , ϕ_B , ϕ_C , and ϕ_r are the absolute phases at the three antennas of the reference triangle and at the reference antenna r , respectively. We then consider the phase for the interpolated or extrapolated antenna t . The absolute and the observed phases for the antenna t can be expressed as ϕ_t and ϕ_{tr} , respectively, and the relation between ϕ_t and ϕ_{tr} can be written as

$$\phi_{tr} = \phi_t - \phi_r. \quad (8)$$

Now, we re-define the phase, which is, not measure from the reference antenna r , but from the center of the triangle (see figure 6b). First, we define $\bar{\phi}$ as

$$\begin{aligned} \bar{\phi} &\equiv \frac{1}{3}(\phi_{Ar} + \phi_{Br} + \phi_{Cr}) \\ &= \frac{1}{3}(\phi_A + \phi_B + \phi_C) - \phi_r. \end{aligned} \quad (9)$$

We can consider this phase as the phase of the center of the triangle relative to the reference antenna r . If we subtract the phase $\bar{\phi}$ from other phases, these phases will be the phases refer to the center of the triangle: For example, the phase of antenna t relative to the center of the reference triangle can be expressed as

$$\phi_{tr} - \bar{\phi} = \phi_t - \phi_r - \bar{\phi}. \quad (10)$$

If we substitute $\bar{\phi}$ in equation (9) into this equation, the equation can be written as

$$\begin{aligned} \phi_{tr} - \bar{\phi} &= \phi_t - \phi_r - \left[\frac{1}{3}(\phi_A + \phi_B + \phi_C) - \phi_r \right] \\ &= \phi_t - \frac{1}{3}(\phi_A + \phi_B + \phi_C). \end{aligned} \quad (11)$$

The final form of this equation does not include the phase of the reference antenna ϕ_r , and only depends on the absolute phase of the target antenna ϕ_t relative to the absolute phase of the center of the triangle, $(\phi_A + \phi_B + \phi_C)/3$.

3.3. Comparison between Actual and Subtracted Phase Fluctuations

We then compare the relationship between the distance from the interpolated/extrapolated antennas to the center of the reference triangle and the subtracted/unsubtracted (corrected/uncorrected) root mean square (rms) of the phase fluctuation, which is depicted in figure 7. We separated the interpolated and the extrapolated antennas, and also separated the large and small phase fluctuation data for each dataset (see table 2). The uncorrected (observed) phase fluctuations are similar or increase with the distance from the center of the reference triangle. The corrected (subtracted) phase, on the other hand, shows different behavior between the interpolated and extrapolated results.

The interpolated results show improvement in phase fluctuation, especially for the longer distance antennas, and in most cases, rms phase turned to be constant, or sometimes better in the longer distance antennas than the shorter distance antennas. This suggests that the phase correction efficiency depends mainly on the distance; better phase correction efficiency at longer distance. This may be because the longer distance antennas are closer to an edge of a reference triangle, namely close to a baseline of two reference antennas (i.e., one dimension), and the

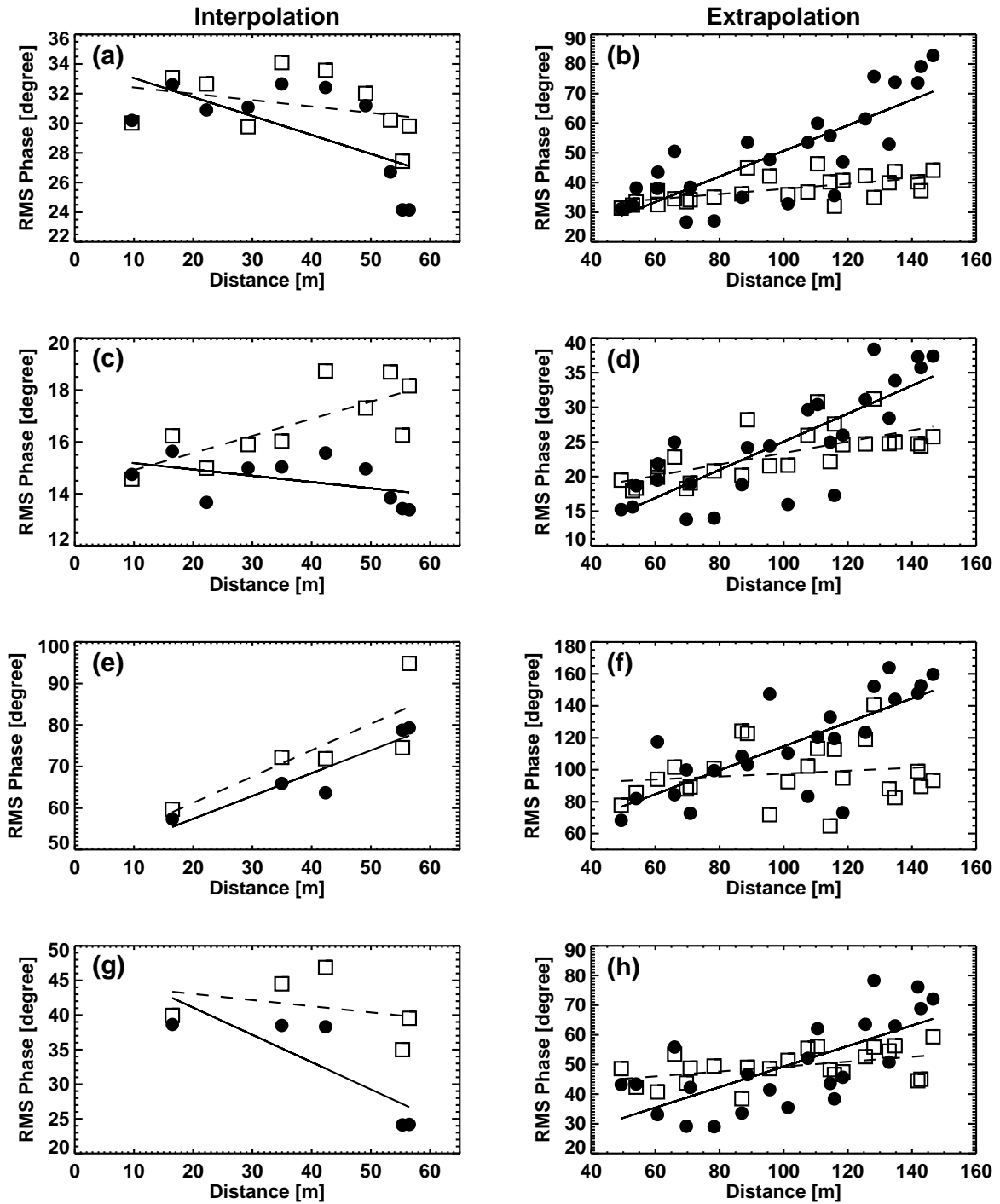


Fig. 7. RMS phase plots of the uncorrected (observed; open squares) and corrected (subtracted; filled circles) phases for the interpolated and extrapolated antennas. Dashed and solid lines are the linear fittings of the uncorrected and corrected phases, respectively. Plots in the left column are the interpolated results, and those in the right column are the extrapolated results. (a) Interpolated results for the integration number range 2321 – 2799 of the dataset 040826. (b) Extrapolated results for the integration number range 2321 – 2799 of the dataset 040826. (c) Interpolated results for the integration number range 2800 – 3128 of the dataset 040826. (d) Extrapolated results for the integration number range 2800 – 3128 of the dataset 040826. (e) Interpolated results for the integration number range 140 – 199 of the dataset 040907. (f) Extrapolated results for the integration number range 140 – 199 of the dataset 040907. (g) Interpolated results for the integration number range 200 – 467 of the dataset 040907. (h) Extrapolated results for the integration number range 200 – 467 of the dataset 040907.

estimated phase turns to be closer to the real phase than the two dimension case (i.e., estimating phase close to the center of the reference triangle with three antennas).

Exception for this result is the earlier part (the integration number range of 140 – 199) of the dataset 040907 (figure 7e; see also figure 4a), which is largely affected by the 2π ambiguity. This interpolation result suggests that the phase correction scheme for the ACA will work properly, as far as the phase does not fluctuate too large ($< 2\pi$).

The extrapolated results, on the other hand, show improvement in some cases, but often turn to be worse. Generally, the phase fluctuation increases with the distance from the center of the reference triangle. This indicates that the extrapolation of the phase screen does not work well for the phase correction. There are huge rises of the corrected phases around the distance of 140 m from the center of the reference triangle in all the extrapolation results (see figures 7b, d, f, and h; compare with the observed rms phases, the corrected rms phases increase significantly). These data points are mostly the extrapolated phases of the antennas 2, 3, and 5 from the reference triangle [2, 4, 6], [2, 4, 7], [3, 4, 6], and [4, 5, 6]. We will discuss this later in section 4.3.

3.4. Comparisons of RMS Phase with Temporal Structure Function

To characterize the tropospheric fluctuation, the structure function (Tatarskii 1961) is often used. Here, to evaluate the time variation of phase quantitatively, we use the temporal structure function, $D_\phi(\tau)$, which can be defined as

$$D_\phi(\tau) \equiv \langle [\Phi(t + \tau) - \Phi(t)]^2 \rangle, \quad (12)$$

where τ is the characteristic integration time interval (in our data, this corresponds to the integration number interval), and $\Phi(t)$ is the phase at integration time t . The angle bracket “ $\langle \rangle$ ” means the time ensemble. We denote ϕ_{rms} as the rms of the temporal structure function $\sqrt{D_\phi}$. We compare ϕ_{rms} of the corrected and uncorrected phase for the interpolated and extrapolated data as a function of integration time intervals. We show some examples in figure 8, which displays the temporal structure functions before and after the interpolation scheme on the antenna 1 and that in the extrapolation scheme on the antenna 3 with the reference triangle [2, 4, 6]. The plots show that rms phase (corresponds to ϕ_{rms} above) rises to a maximum value as integration number interval (corresponds to τ in the equation 12) increases, and tend to be flat at this maximum value. If the maximum value for the corrected phase turns to be lower than the uncorrected phase, the temporal structure function plots tell that the phase correction worked well. The interpolation scheme improves the phase, while the extrapolation scheme makes the phase fluctuation worse.

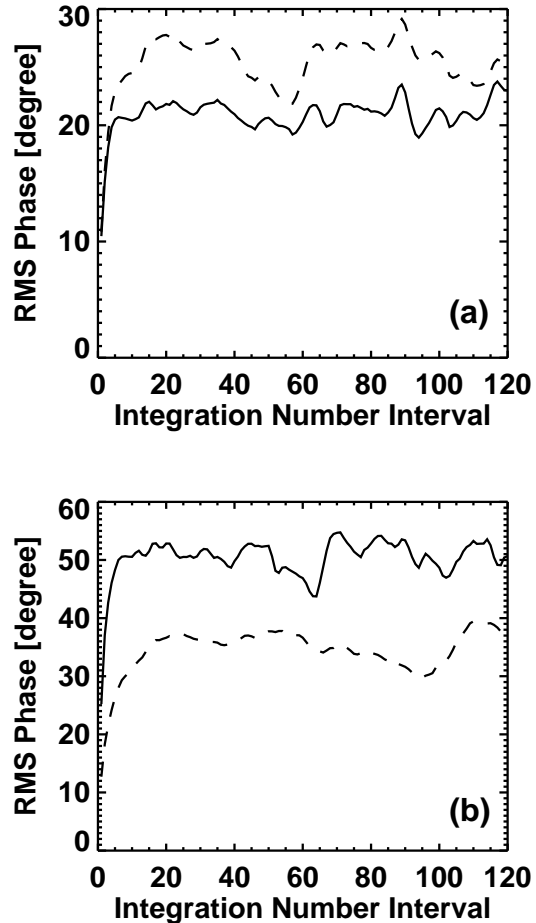


Fig. 8. Examples of the temporal structure function plots for the corrected (solid lines) and uncorrected (dashed) rms phases with the reference triangle [2, 4, 6] from the dataset 040826. (a) The interpolated antenna 1 temporal structure function plots for the integration number range 2800 – 3128. (b) The extrapolated antenna 3 temporal structure function plots for the integration number range 2800 – 3128.

4. Discussion

In the previous section, we showed that the interpolation phase correction scheme worked well in our experiments, which supports the use of this scheme for the ACA. Here we discuss the possible explanations for the success of the interpolation scheme and failure of the extrapolation scheme, the application of our results to the ACA phase correction scheme, and the validity of the “frozen-flow” model.

4.1. Interpolation and Extrapolation Phase Correction Schemes

The results of our experiments exhibit that the interpolation scheme provides a better phase correction than the extrapolation approach. The difference between these two schemes can be compared in figure 9 (simplified to one-dimensional example). The interpolation scheme is cal-

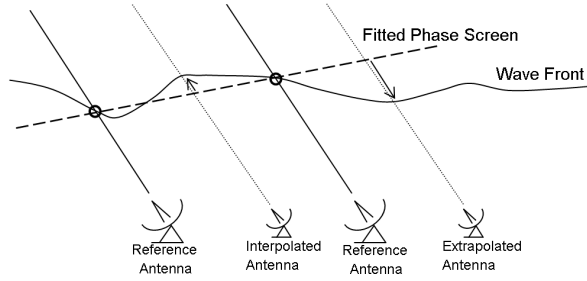


Fig. 9. The wavefront corrected by the fitted phase screen. Under this one-dimensional example, the interpolation estimations have two reference antennas being “two-side” boundary condition, while the extrapolation estimations have only “one-side” boundary condition.

culated under the three boundary conditions of the three antenna phases surrounding the antennas to be corrected, while the extrapolation scheme is calculated for antennas outside a reference triangle, namely only one boundary condition on one side, and no boundary condition on the other sides. Therefore, the extrapolation results deviate more than the interpolation results due to more degrees of freedom or more uncertainties. Furthermore, the distortion of the wave front is caused by the variations of the water vapor distribution in the troposphere that move across an interferometer. The situation between the atmosphere and the interferometer is depicted in figure 10. Smaller scale water vapor “clumps” cause a smaller phase variations, and larger scale “clumps” cause a larger phase variations. In case of the interpolation scheme, the water vapor clumps larger than the separation of the reference antennas can be corrected by the phase screen, and only the small fluctuation remains.

On the other hand, since the extrapolation scheme is calculated with only one boundary condition, the water vapor clumps detected with the reference triangle may not be related to that detected with the extrapolated antennas, and therefore resulted as a large variation of phase (larger the distance from the center of the reference triangle, larger the phase variations; but see section 4.3 for the difference in the phase correction results between the antennas located along or perpendicular to the wind direction from the reference triangle).

4.2. Differences between Our Experiments and the ACA Phase Correction Scheme

Although our results support the ACA phase correction scheme, there are some differences between our experiments and the proposed scheme. One is the difference in sites; our experiments were done at the summit of Mauna Kea, Hawaii, but the ALMA site is located at Chajnantor, Chile. Therefore the atmospheric conditions between these two sites may have different characteristics. However, past several site testing results using radio seeing monitors indicate that the structure functions, which characterizes the water vapor clumps in the atmosphere, of these two sites do not differ much (Holdaway et al.

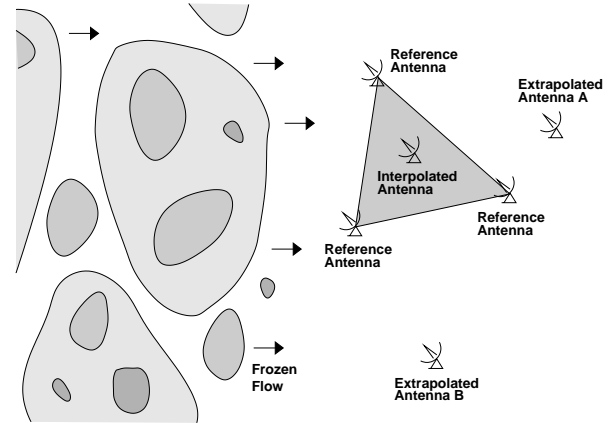


Fig. 10. Schematic diagram showing the antenna configurations and the frozen flow of water vapor clumps.

1995). Hence this point will not be a problem.

The other is the difference in the antenna configuration of our tests and the actual configuration of the WVRs in the ACA, namely the configuration of a phase screen. Our experiments uses three antennas to create a phase screen, and therefore one phase plane is naturally created without any offset from measured phases. The ACA, however, uses four WVRs, so that a fitting is needed to create a phase screen, which produces some difference between the measured phases and the estimated phase screen. This difference may create some errors in the phase correction, which leads to larger phase fluctuations after the correction than our results. Indeed, as mentioned in section 3.3, the phase correction works better near the edge of the reference triangle (i.e., near one baseline), supporting this concern. It would be the future study to compare the phase correction results using phase screens derived from three antennas and that from four antennas.

4.3. Extraordinary 140 m Phase Fluctuations

In general cases, the phase fluctuation gradually increases with the increase of distance from the center of the reference triangle to the interpolated or extrapolated antennas in our experiments. However, as mentioned in section 3.3, the corrected phases of the extrapolation scheme suddenly rise up around the distance from the center of the reference triangle of 140 m, much more (almost twice worse) than the original observed phase fluctuation.

The large scatter is possibly due to the orientation (direction) of the center of the reference triangle to the extrapolated antennas. Figure 11 presents an example configuration of the reference triangle [2, 4, 6] for the extraordinarily large rms phase fluctuation data point for the antenna 3. The extraordinary 140 m phase fluctuation data all have similar orientation, which is almost along the north-south direction. The meteorological parameters on the two observation days show that the prevailing wind direction is either east or west. This wind direction is almost perpendicular to the orientations of the antenna configurations with the extraordinary 140 m fluctuations

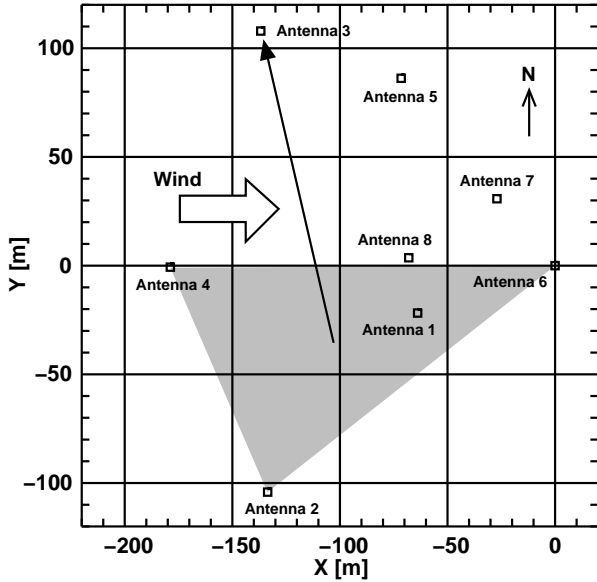


Fig. 11. Schematic diagrams of phase screens created by reference antennas and the distance from the center of the reference triangle to the extrapolated antennas. The black arrow shows an example of the extrapolated antenna 3 with the distance from the center of the reference triangle [2, 4, 6] of around 140 m. The white arrow is the rough direction of the prevailing wind of an observed day.

on both days (figure 11).

A possible explanation for this extraordinary phenomenon is as follows: The time variations of the atmospheric phase are usually approximated by a “frozen-flow” model (Taylor 1938; Dravskikh & Finkelstein 1979): The time scale to develop/cease a turbulence is much longer than the time taken for a turbulent field to pass across the reference triangle by wind. Hence the turbulence of water vapor is generally ‘frozen’ in the atmosphere, and the wind transport the water vapor turbulences above an interferometer without changing the size of the turbulences (figure 10). Under this “frozen-flow” hypothesis, the antennas outside the reference triangle but along the wind direction (for example, the extrapolated antenna A in figure 10), the observed phase will not be largely different from the estimated phase by the extrapolation of the phase screen, since the water vapor turbulences that pass in front of the antennas are similar to that pass in front of the reference triangle. Therefore the phase fluctuation after the phase correction gradually increases with the distance from the center of the reference triangle. Indeed, some of the corrected phases for the extrapolated antennas are improved from the uncorrected phases (see figure 7), and most of those extrapolated antennas are located along the wind direction from the reference triangles. However, the antennas outside the reference triangle but perpendicular to the wind direction (for example, the extrapolated antenna B in figure 10), the observed phase will be largely different from the estimated phase by the extrapolation of the phase screen, since the water vapor turbulences that pass in front of the antennas are different from that pass in

front of the reference triangle. Therefore the phase fluctuation after the phase correction generally make results worse.

The location between the antennas that caused the “140 m phase fluctuation” and the center of the reference triangle is almost perpendicular to the wind direction of the observed days, and other antennas are along the wind direction. We therefore conclude that the results of the extrapolation scheme including the “140 m phase fluctuation” can be explained by “frozen-flow” model.

5. Conclusions

We performed an interferometric phase correction with the interpolation or extrapolation of the phase screen defined by three reference antennas using the SMA. This interpolation method is proposed for the ACA in the ALMA.

According to the comparisons of the standard deviations of corrected and uncorrected phases, relations between the phase standard deviation and the distance from the center of the reference triangle, and the temporal structure functions of the rms phase, the interpolation scheme improves phase fluctuation while the extrapolation scheme does not. This result can be explained by the boundary conditions of phase in these schemes; in case of the interpolation scheme, the phase corrected antenna is inside the triangle of three reference antennas, so the phase inside the triangle can be well defined (more known boundary conditions, more precisions or less phase errors and deviations). The extrapolation scheme, on the other hand, only has partial boundary conditions, and therefore less precision.

In the extrapolation scheme results, there is a sudden large phase fluctuation at the distance from the center of the reference triangle of about 140 m. According to the meteorological parameters on those observing dates and the antenna configurations, this “140 m phase fluctuation” is occurring only at the antennas located from the center of the reference triangle perpendicular to the wind direction. This “140 m phase fluctuation” can be explained by the frozen-flow model.

Although there are some differences between the configuration of our experiments and that in the proposed phase correction scheme for the ACA, our results based on the actual observations and the simulation results done by Asaki et al. (2005) promise the success of the phase correction for the ACA.

We would like to thank Kazushi Sakamoto and Koh-ichiro Morita for fruitful discussion. The Submillimeter Array is a joint project between the Smithsonian Astrophysical Observatory and the Academia Sinica Institute of Astronomy and Astrophysics and is funded by the Smithsonian Institution and the Academia Sinica.

References

- Asaki, Y., Saito, M., Kawabe, R., Morita, K.-I., & Sasao, T. 1996, *Radio Science*, 31, 1615
- Asaki, Y., Shibata, K. M., Kawabe, R., Roh, D. G., Saito, M., Morita, K.-I., & Sasao, T. 1998, *Radio Science*, 33, 1297
- Asaki, Y., Saito, M., Kawabe, R., Morita, K.-I., Tamura, Y., & Vila-Vilaro, B. 2005, *ALMA Memo* 535
- Butler, B. J., Radford, S. J. E., Sakamoto, S., & Kohno, K. 2001, *ALMA Memo*, 365
- Carilli, C. L., & Holdaway, M. A. 1997, *ALMA Memo* 173
- Carilli, C. L., & Holdaway, M. A. 1999, *Radio Science*, 34, 817
- Carilli, C. L., Holdaway, M. A., & Ishiguro, M. 1996, *VLA Scientific Memo* 171
- Carilli, C. L., Lay, O., & Sutton, E. C. 1998, *ALMA Memo* 210
- Delgado, G., et al. 2000, *ALMA Memo* 332
- Dravskikh, A. F., & Finkelstein, A. M. 1979, *Ap&SS*, 60, 251
- Ho, P. T. P., Moran, J. M., & Lo, F. 2004, *ApJL*, 616, L1
- Holdaway, M. A. 1992, *ALMA Memo* 84
- Holdaway, M. A., Matsushita, S., & Saito, M. 1997, *ALMA Memo*, 176
- Holdaway, M. A. & Owen, F. N. 1995, *ALMA Memo* 126
- Holdaway, M. A., Radford, S. J. E., Owen, F. N., & Foster, S. M. 1995, *ALMA Memo* 139
- Iguchi, S., et al. 2009, *PASJ*, 61, 1
- Lay, O. P. 1997, *A&AS*, 122, 547
- Marvel, K., & Woody, D. 1998, *Proc. SPIE*, 3357, 442
- Matsuo, H., Sakamoto, A., & Matsushita, S. 1998, *PASJ*, 50, 359
- Matsushita, S., & Matsuo, H. 2003, *PASJ*, 55, 325
- Matsushita, S., Matsuo, H., Pardo, J. R., & Radford, S. J. E. 1999, *PASJ*, 51, 603
- Matsushita, S., Matsuo, H., Wiedner, M. C., & Pardo, J. R. 2002, *ALMA Memo* 415
- Morita, K.-I., Handa, K., Asaki, Y., Kitamura, Y., Yokogawa, S., Saito, M., Wilner, D. W., & Ho, P. T. P. 2000, *ASP Conf. Ser.*, 217, 340
- Paine, S., Blundell, R., Papa, D. C., Barrett, J. W., & Radford, S. J. E. 2000, *PASP*, 112, 108
- Radford, S. J. E., Reiland, G., & Shillue, B. 1996, *PASP*, 108, 441
- Tatarskii, V. I. 1961, *Wave Propagation in a Turbulent Medium* (New York: Dover)
- Taylor, G. I. 1938, *Proc. Roy. Soc. London Ser. A*, 164, 476
- Thompson, A. R., Moran, J. M., & Swenson, G. W. 2001, *Interferometry and Synthesis in Radio Astronomy* (New York: John Wiley & Sons), 507
- Wiedner, M. C., Hills, R. E., Carlstrom, J. E., & Lay, O. P. 2001, *ApJ*, 553, 1036
- Wooten, A., & Thompson, A. R. 2009, *Proc. IEEE*, 97, 1463